Rapid Communications

Nonlocal shear-thinning effects substantially enhance helical propulsion

Ebru Demir,[1,2] Noah Lordi,[2] Yang Ding,[1,*] and On Shun Pak[2,†]
[1]*Mechanics Division, Beijing Computational Science Research Center, Haidian, Beijing, China*
[2]*Department of Mechanical Engineering, Santa Clara University, Santa Clara, California 95053, USA*

(Received 9 August 2020; accepted 16 October 2020; published 11 November 2020)

Helical propulsion is ubiquitously adopted by swimming bacteria and artificial microswimmers to move in biological fluids, which are typically viscoelastic and shear thinning. Here we present a set of theoretical and computational analyses to show that shear-thinning viscosity alone can cause the substantial enhancement reported for helical propulsion in recent experiments. Our analyses provide direct evidence to elucidate the nonlocal nature of the enhancement mechanism. Since the enhancement predicted here can be more substantial than that due to viscoelasticity, our results also suggest that shear-thinning rheology may play a more dominant role in the observed enhancement of bacterial motility in polymeric fluids.

DOI: 10.1103/PhysRevFluids.5.111301

Helical shapes are ubiquitous in natural and artificial structures. Bacteria such as *Escherichia coli* and *Vibrio alginolyticus* exploit the rotation of their helically shaped flagella to swim through the microscopic world, similar to the motion of a corkscrew when opening a bottle of wine [1,2]. This propulsion strategy has also inspired the development of artificial helical propellers [3,4], which are helical microstructures that propel upon an imposed rotating magnetic field. These artificial microswimmers have shown great promise in various biomedical applications such as drug delivery and microsurgery [5]. For its ubiquity as a biological and artificial propulsion mechanism, helical locomotion has been studied in diverse media, from purely viscous (Newtonian) fluids [6–8] and porous media [9], to more complex environments such as granular media [10] and non-Newtonian (complex) fluids [11,12]. In particular, enhanced bacterial locomotion observed in complex fluids has attracted substantial attention [13–16]. Continual efforts strive to seek a better understanding of the physical mechanisms underlying the enhancement [9,17–21], which could also guide the design of artificial microswimmers in biological fluids [22].

Biological fluids typically display complex rheological properties including viscoelasticity and shear-thinning rheology [23,24]. A viscoelastic fluid exhibits elastic characteristics, whereas the viscosity of a shear-thinning fluid decreases with the shear rate. While extensive studies focused on fluid elasticity [11,12,25–30], the shear-thinning effect has been largely overlooked until more recently [31]. Since shear-thinning viscosity impacts both thrust and drag simultaneously in nontrivial manners, its overall effect on propulsion is not obvious. Moreover, although a drag and thrust decomposition can provide insights into locomotion in Newtonian fluids, one should use caution when extending this intuition to locomotion in non-Newtonian media due to the nonlinearity in the constitutive equation [32]. Whether the shear-thinning rheology enhances or hinders locomotion can largely depend on the type of swimmers and details of their swimming gaits: For undulatory swimmers, theoretical and numerical studies [33–35] together with experiments

*dingyang@csrc.ac.cn
†opak@scu.edu

on nematodes [36,37] showed that they can display equal or faster than Newtonian swimming in shear-thinning fluids, depending on the amplitude of undulation; a cautionary note was also made on the difference between two-dimensional (2D) versus three-dimensional (3D) undulatory swimmers in shear-thinning fluids [38]. For squirmers, while neutral squirmers, pushers and pullers swim slower in shear-thinning fluids [32,33], speed enhancement is possible when higher squirming modes are present in the surface velocities [32].

In this work, we focus on the effect of shear-thinning rheology on helical propulsion, a ubiquitous mechanism adopted by swimming bacteria and artificial microswimmers. Recent experiments on helical propellers driven by an external rotating magnetic field (up to 10 Hz) reported considerably faster propulsion speeds in fluids displaying shear-thinning behaviors (for steady shear rates ranging from 0.1 to 100 s^{-1}) than in Newtonian fluids: The speed enhancement is among the strongest (up to 50% faster than the Newtonian speed) of such type reported to date [40]. However, such a substantial enhancement has not yet been investigated theoretically, and the underlying mechanism remains unclear. In this work, we present a first set of theoretical analysis and simulations to show that shear-thinning rheology, alone, can indeed cause the substantial enhancement reported for helical propulsion in the experiments [40]. Our analyses here provide direct evidence to confirm the nonlocal nature of the underlying enhancement mechanism. In addition, by comparison with the enhancement due to fluid elasticity [11,12], our results suggest that the shear-thinning effect may play a more dominant role in the observed enhancement of bacterial locomotion in polymeric fluids [13–16,41]. We present our analyses below.

In general, shear-thinning rheology can impact locomotion in both local and nonlocal manners [35,42]: While the local effect of viscosity reduction due to increased shear rates alters the local stress distribution on a swimmer, the modified stress balance also induces (nonlocal) overall changes to the flow around the swimmer. The relative importance of these local and nonlocal effects may vary among different types of swimmers [35,40,42,43]. A recent framework based on a modified resistive force theory (RFT) in a shear-thinning fluid has focused only on the local effect but obtained reasonable agreement with experimental measurements on undulatory swimmers [42]. Here we adopt the same framework to probe the local shear-thinning effect on helical propulsion.

To construct a theoretical model, we consider a helical structure of infinite length with the centerline expressed in terms of the arc length s and time t as $\mathbf{x}(s,t) = R\cos(ks+\Omega t)\hat{\mathbf{e}}_x + R\sin(ks+\Omega t)\hat{\mathbf{e}}_y + (s\cos\theta + Ut)\mathbf{e}_z$; here R is the helix radius, $k = 2\pi/\Lambda$ with Λ representing the arc length of a single helical turn, θ is the pitch angle, Ω is a constant rotation speed, and U is the resulting propulsion speed [Fig. 1(a)]. With the biologically relevant assumption that the filament is slender (the filament radius $a \ll$ the filament length L), the force density along the filament $\mathbf{f}$ depends only on the local velocity $\mathbf{u}$ in a purely viscous liquid to leading order as described by the local RFT [44–46]. Riley and Lauga [42] proposed a modified RFT for locomotion of slender bodies in shear-thinning fluids as $\mathbf{f} = -R_C[\xi_\parallel \mathbf{tt} + \xi_\perp(\mathbf{I}-\mathbf{tt})]\cdot\mathbf{u}$, where $\mathbf{t} = \mathbf{x}_s$ is the local unit tangent vector and $\mathbf{I}$ is the identity tensor. Here the coefficients $\xi_\parallel = 2\pi\mu/[\ln(L/a) - 1/2]$ and $\xi_\perp = 4\pi\mu/[\ln(L/a) + 1/2]$ are given by classical RFT results in a purely viscous liquid [44–46] and R_C is a correction factor accounting for the local shear-thinning effect. Based on the Carreau constitutive model with a critical shear rate $1/\lambda_C$ [42,47], Riley and Lauga proposed the correction factor $R_C = [1 + (\lambda_C\dot{\gamma}_{\text{avg}})^2]^{(n-1)/2}$, where the local average shear rate around a cylinder $\dot{\gamma}_{\text{avg}} = \sqrt{\xi_\perp^2 u_\perp^2 + 2\xi_\parallel^2 u_\parallel^2}/(2\sqrt{2}a\pi\mu_0)$ can be calculated with the local tangential ($u_\parallel = |\mathbf{t}\cdot\mathbf{u}|$) and normal ($u_\perp = |(\mathbf{I}-\mathbf{tt})\cdot\mathbf{u}|$) velocity components. In general, the magnitude of the velocity components ($u_\parallel$ and $u_\perp$) and thus the local shear rate vary along a swimming body. The force density $\mathbf{f}$ is therefore modified through the spatially and temporally dependent correction factor R_C. Such modifications were shown to cause slower swimming speeds in a shear-thinning fluid than in a Newtonian fluid for undulatory swimmers [42]. For helical propulsion considered here, in contrast, the magnitude of the velocity components and hence the local shear rate do not vary along a rotating helix due to symmetry of the helical body and the imposed axial rotation. In other words, the local shear-thinning effect alters the force density on the swimmer uniformly through a spatially and temporally

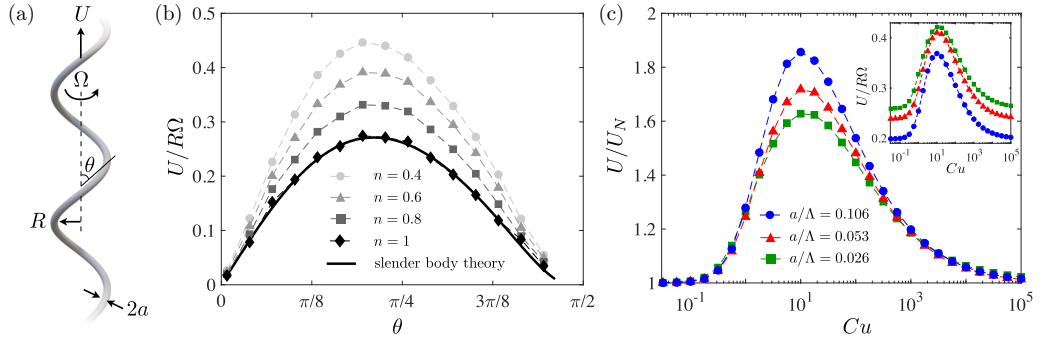

FIG. 1. (a) Schematic of a helical body of infinite length rotating about its axis at a prescribed rotation rate, Ω, and propelling at a speed, U, along the axis. (b) The scaled propulsion speed $U/R\Omega$ as a function of the pitch angle θ in shear-thinning fluids with different values of power index n, at a fixed Carreau number $\mathrm{Cu} = 10$, viscosity ratio $\mu_\infty/\mu_0 = 0.1$, and filament aspect ratio (or slenderness) $a/\Lambda = 0.026$. The value of slenderness considered here is obtained from helical filaments used in previous experiments [11]. In the Newtonian limit ($n = 1$), the computational model shows excellent agreement with results based on Lighthill's slender-body theory [39] and experimental results in Ref. [11]. (c) The non-Newtonian propulsion speed relative to the Newtonian speed U/U_N as a function of Cu for different values of filament slenderness a/Λ. There exist optimal values of Cu maximizing the speed, with more pronounced enhancement (relative to the corresponding Newtonian value) for a thicker filament ($a/\Lambda = 0.106$; more than 80%) than thinner filaments. Here $\mu_\infty/\mu_0 = 0.1$ and $n = 0.4$. Inset: the scaled propulsion speed as a function of Cu.

independent correction factor R_C. The resulting total force on the swimmer is hence given by $\int_0^L \mathbf{f}_C ds = R_C \int_0^L [\xi_\parallel \mathbf{tt} + \xi_\perp(\mathbf{I} - \mathbf{tt})] \cdot \mathbf{u}\, ds$, where the correction factor R_C can be moved outside of the integral for helical propulsion. Upon enforcing the overall force-free condition ($\int_0^L \mathbf{f} ds = \mathbf{0}$), the effect due to the correction factor vanishes as R_c gets divided out. The resulting force balance is therefore the same as the Newtonian case: $\int_0^L [\xi_\parallel \mathbf{tt} + \xi_\perp(\mathbf{I} - \mathbf{tt})] \cdot \mathbf{u}\, ds = \mathbf{0}$, yielding a propulsion speed same as that in a Newtonian fluid. Unlike undulatory swimmers, the RFT analysis above concludes that the local shear-thinning effect does not alter the propulsion speed of a rotating helix. This result may be interpreted as that the local shear-thinning effect modifies the drag and thrust components on the helix by the same amount, leaving zero net effect on their balance. To conclude, the local analysis fails to capture the substantially enhanced helical propulsion in a shear-thinning fluid observed in recent experiments [40], suggesting the crucial role of nonlocal shear-thinning effects on this mode of propulsion.

To fully capture the shear-thinning effects, we use finite-element analysis and solve the momentum equation in the inertialess regime, $\nabla \cdot \mathbf{T} = \mathbf{0}$, for the incompressible flow ($\nabla \cdot \mathbf{u} = 0$) around the helix. The stress tensor is given by $\mathbf{T} = -p\mathbf{I} + \boldsymbol{\tau}$, where p is the pressure and the deviatoric stress is given by the Carreau constitutive equation [47]

$$\boldsymbol{\tau} = \left[\mu_\infty + (\mu_0 - \mu_\infty)\left(1 + \lambda_C^2 |\dot{\boldsymbol{\gamma}}|^2\right)\right]^{(n-1)/2} \dot{\boldsymbol{\gamma}}, \tag{1}$$

where μ_0 and μ_∞ represent the zero and infinite-shear rate viscosities, respectively, and the strain rate tensor $\dot{\boldsymbol{\gamma}} = \nabla\mathbf{u} + (\nabla\mathbf{u})^T$ with its magnitude given by $|\dot{\boldsymbol{\gamma}}| = (\dot{\gamma}_{ij}\dot{\gamma}_{ij}/2)^{1/2}$. The power law index $n < 1$ characterizes the degree of shear thinning, and $1/\lambda_C$ characterizes the critical shear rate at which the non-Newtonian behavior becomes significant. The Carreau number $\mathrm{Cu} = \lambda_C \Omega$ compares the rotation rate of the helix to the critical shear rate of the shear-thinning fluid. By imposing the rotation rate on the helix through a boundary condition, we solve numerically the flow and stress fields surrounding the helix and enforce the force-free condition along the axial direction to determine the resulting axial swimming speed, U. We perform the finite-element analysis in the COMSOL Multiphysics environment with periodic boundary conditions on the ends of a single helical

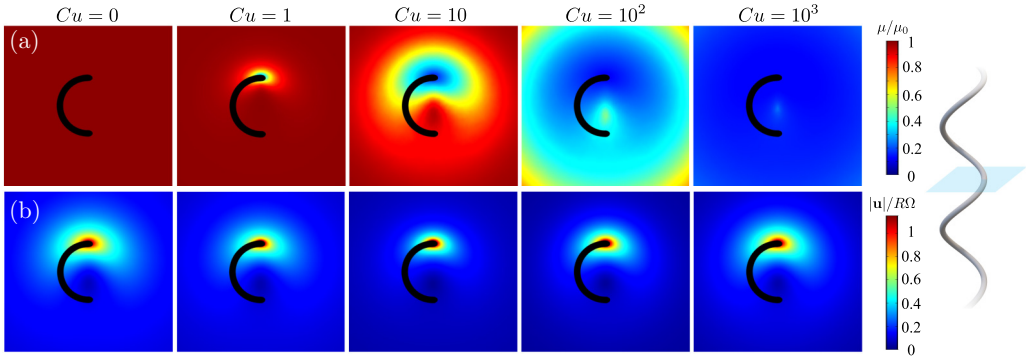

FIG. 2. The distribution of viscosity and flow speed on a cross section of the rotating helix at varying Cu. (a) The scaled viscosity distribution, μ/μ_0, around the rotating helix. (b) The corresponding scaled flow speed distribution, $|\mathbf{u}|/R\Omega$, around the rotating helix. The cross section is taken on the midplane with a normal in the direction of propulsion (see the schematic on the right). In each distribution, only a half helical turn of the helix (out of the plane) is depicted. Here $\theta = \pi/4$, $a/\Lambda = 0.026$, $\mu_\infty/\mu_0 = 0.1$, and $n = 0.4$.

turn to simulate a rotating helix of infinite length. We use a cylindrical computational domain of a radius $1000(R + a)$ with the degree of freedom on the order of 10^5-10^6 depending on the pitch angle. The mesh near the helix is locally refined to properly capture the spatial variation of the viscosity. We use the MUMPS (Multifrontal Massively Parallel Sparse) direct solver for all simulations. We validate the computational model against results in the Newtonian limit based on Lighthill's slender body theory [39] (black solid line) by setting $n = 1$ in the simulation [black diamonds, Fig. 1(b)]; the numerical and theoretical results show excellent agreement.

We then use the computational model to examine how shear-thinning rheology affects helical propulsion by reducing the power index n from unity at fixed Cu $= 10$ and viscosity ratio $\mu_\infty/\mu_0 = 0.1$. As shown in Fig. 1(b), the propulsion speed of the rotating helix increases as the fluid becomes more shear thinning (i.e., as n decreases). We remark that the optimal pitch angle for helical propulsion in a shear-thinning fluid does not deviate significantly from the Newtonian value. Next, we examine how the scaled propulsion speed varies with the dimensionless rotation rate, Cu, for different values of filament aspect ratio (or slenderness), a/Λ [Fig. 1(c) inset]. The variation is nonmonotonic: The speed first increases from its Newtonian value (U_N) with Cu and reaches a maximum speed when Cu ≈ 10, before decreases at larger Cu. The propulsion speed is consistently enhanced relative to the Newtonian speed, $U/U_N > 1$, for a wide range of Cu shown in Fig. 1(c). While the speed generally increases as the filament becomes more slender [Fig. 1(c) inset], the enhancement relative to the Newtonian value is more pronounced for a thicker filament than the thinner filaments [Fig. 1(c)]. The maximum enhancement can range from approximately 60% to more than 80% for the values of slenderness examined here. The substantial increase in propulsion speed is consistent with the order of magnitude measured in the experiment [40] and is considerably larger than that due to fluid elasticity (typically less than 20% [11,12]). Since the RFT analysis concludes that the local shear-thinning effect does not alter the propulsion, the substantial enhancements predicted here should be attributed to a nonlocal mechanism that we discuss next.

The generation of propulsion by slender filaments in the Stokes regime relies on the presence of drag anisotropy [48,49] ($\xi_\perp/\xi_\parallel > 1$), which is known to increase near a confining surface [50,51]. The confinement effect can hence increase the propulsion speed of a rotating helix near a planar wall [52]; enhanced helical propulsion was also found inside a cylinder in a Newtonian fluid [53,54]. The way locomotion is enhanced in a shear-thinning fluid has been hypothesized to be akin to that due to confinement [35,40]: In a shear-thinning fluid, the swimmer's actuation is expected to induce higher shear rates and hence lower viscosities in its nearby regions, which are then encompassed by fluid with higher viscosities. The swimmer hence creates a "soft" confinement around itself, in a fashion

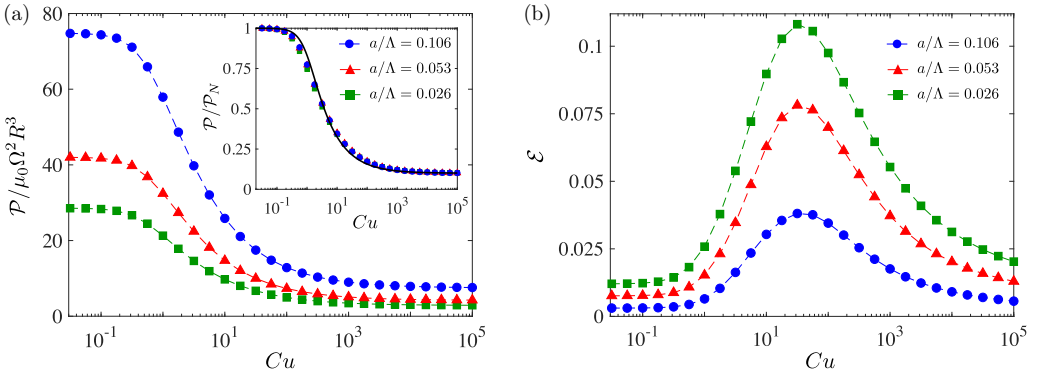

FIG. 3. The energetic cost of helical propulsion in a shear-thinning fluid. (a) The scaled power expended by the rotating helix during propulsion $\mathcal{P}/\mu_0\Omega^2R^3$ as a function of Cu for different values of filament slenderness a/Λ. Inset: the power consumption relative to the corresponding Newtonian value $\mathcal{P}/\mathcal{P}_N$ as a function of Cu; results based on different values of filament slenderness all collapse reasonably well onto the curve describing the viscosity variation given by the Carreau model [Eq. (1) with $|\dot{\boldsymbol{\gamma}}| = \Omega$]: $\mu/\mu_0 = \mu_\infty/\mu_0 + (1-\mu_\infty/\mu_0)(1+\mathrm{Cu}^2)^{(n-1)/2}$ (black solid line). (b) The propulsion efficiency $\mathcal{E}$ of the rotating helix in a shear-thinning fluid for different values of filament slenderness a/Λ. The efficiency is consistently enhanced for a wide range of Cu shown, with maximum efficiency occurring at $\mathrm{Cu} = O(10)$; the enhancement can be more than tenfold compared with the Newtonian efficiency ($\mathrm{Cu} = 0$).

similar to that occurs for undulatory swimmers [35,42]. We examine this soft confinement effect on helical propulsion at varying Cu in Fig. 2. As Cu increases, both the magnitude of viscosity reduction and the size of the low-viscosity region increase. While a more substantial viscosity reduction leads to a stronger soft confinement effect, an increased size of the low-viscosity region makes the swimmer less confined. These two competing effects give rise to an optimal $\mathrm{Cu} = O(10)$ that results in a low-viscosity region of an intermediate size with steep viscosity gradients surrounding the helix [Fig. 2(a), $\mathrm{Cu} = 10$]. The viscosity gradient affects the spatial decay of the flow away from the helix nonmonotonically with increasing Cu as shown in Fig. 2(b). At the optimal $\mathrm{Cu} = O(10)$, the flow decays the most rapidly away from the helix correspondingly. The low-viscosity region at this Cu is still attached to individual cross sections of the helix, in contrast to the case of $\mathrm{Cu} = 100$, where the entire helix is immersed in an enlarged low-viscosity region; the latter scenario has a stronger resemblance to the case of helical propulsion inside a circular cylinder [53,54]. The more tightly attached (to individual cross sections) soft confinement at $\mathrm{Cu} = 10$ leads to the maximum enhancement in propulsion speed. At even larger Cu [e.g., $\mathrm{Cu} = 1000$ in Fig. 2], the low-viscosity region is so large that the helix is virtually propelling through an unbounded Newtonian fluid with a low viscosity. Since the propulsion speed of a helix rotating at a prescribed rate is independent of its viscosity in a Newtonian fluid [6,9], the propulsion speed decreases and approaches the Newtonian value with increasing Cu; accordingly, the flow field at high Cu is similar to that in the Newtonian case [Fig. 2(b)].

The energetic cost of swimming is another biologically relevant performance measure of locomotion in addition to propulsion speed. We calculate the power expended by a rotating helix during its propulsion, $\mathcal{P} = -\int_S \mathbf{T}\cdot\mathbf{n}\cdot\mathbf{u}\, dS$, which decreases monotonically with increased Cu for different values of filament slenderness as shown in Fig. 3(a). When $\mathcal{P}$ is scaled by the corresponding Newtonian value $\mathcal{P}_N$, all results collapse reasonably well onto a single curve describing the dimensionless viscosity variation based on the Carreau model [Eq. (1) with $|\dot{\boldsymbol{\gamma}}| = \Omega$]: $\mu/\mu_0 = \mu_\infty/\mu_0 + (1-\mu_\infty/\mu_0)(1+\mathrm{Cu}^2)^{(n-1)/2}$ [black solid line, Fig. 3(a) inset]; the collapse attributes the decrease in the power expended primarily to the effect of local viscosity reduction. Next, we calculate the propulsion efficiency introduced by Lighthill [45,55], $\mathcal{E} = \mathcal{P}_d/\mathcal{P}$, which

compares the power required to drag the helical structure at the same propulsion speed through the shear-thinning fluid ($\mathcal{P}_d$, which may be interpreted as the useful power output) to the total power consumption $\mathcal{P}$. Enhanced propulsion efficiency in shear-thinning fluids was reported for the waving sheet and squirmer models [34,56]. For helical propellers, similar to propulsion speed, the propulsion efficiency is also enhanced for a wide range of Cu shown in Fig. 3(b). Although helical propulsion at low Reynolds numbers is known to have typically low efficiency in a Newtonian fluid [7,8], we show here that shear-thinning rheology can substantially increase the efficiency (e.g., by more than tenfold) when Cu is optimized to be $O(100)$ as shown in Fig. 3(b). While fluid elasticity can also increase efficiency of helical propulsion (typically less than 60% [12]), the enhancement caused by shear-thinning viscosity here is among the strongest reported to date.

Taken together, we show that shear-thinning viscosity alone can cause the substantial enhancement reported for helical propulsion in recent experiments [40]. Our theoretical and computational analyses elucidate the nonlocal nature of the mechanism—a soft confinement effect—underlying the enhancement. Since the magnitude of enhancement due to shear-thinning rheology can be considerably larger than that due to viscoelasticity [11,12], our results also suggest that shear-thinning effects could be a major reason for enhanced bacterial swimming speeds in a polymeric fluid, consistent with the conclusion of recent experiments on bacterial motility [41]. We remark that the critical shear rate of biological fluids spans a wide range, with λ_C ranging from a tenth of a second to seconds for blood [57,58] and hundreds of seconds or larger for bile and different mucus [34,59]. For a rotating frequency of the bacterial flagellum on the order of 100 Hz [60], typical Cu may be estimated to be on the order of 100 or higher. To fully capitalize on the non-Newtonian rheology of a specific biological fluid for enhanced propulsion, the rotating frequency of artificial helical propellers can be tuned to achieve the optimal Cu, which occurs at $O(10)$ for speed and $O(100)$ for efficiency. Overall, our results demonstrate the robust performance of helical propulsion as a ubiquitous biological and artificial propulsion strategy in both Newtonian and non-Newtonian media. Finally, we consider in this work the infinite helix model as a first step to understand the effect of shear-thinning rheology on helical propulsion. The results can be directly applied to inform the design of artificial helical propellers that achieve corkscrew locomotion without a head under rotating magnetic fields [61–63]. For biological swimmers that require a head for helical locomotion, shear-thinning rheology will also modify the torque balance between the rotating head and the helical flagellum as well as their hydrodynamic interactions. The impact of these effects, together with the three-dimensional swimming kinematics and end effects of finite-size swimmers, represent some interesting aspects of helical locomotion in shear-thinning fluids to be addressed in future work.

O.S.P. acknowledges support by the National Science Foundation (Grant No. CBET-1931292). Y.D. acknowledges support by the National Science Foundation of China (NSFC-NSAF Grant No. U1930402). Computations were performed using the WAVE computing facility at Santa Clara University, enabled by the Wiegand Foundation.

[1] H. C. Berg, *Random Walks in Biology* (Princeton University Press, Princeton, NJ, 1993).
[2] E. Lauga, Bacterial hydrodynamics, Annu. Rev. Fluid Mech. **48**, 105 (2016).
[3] L. Zhang, J. J. Abbott, L. Dong, K. E. Peyer, B. E. Kratochvil, H. Zhang, C. Bergeles, and B. J. Nelson, Characterizing the swimming properties of artificial bacterial flagella, Nano Lett. **9**, 3663 (2009).
[4] A. Ghosh and P. Fischer, Controlled propulsion of artificial magnetic nanostructured propellers, Nano Lett. **9**, 2243 (2009).
[5] B. J. Nelson, I. K. Kaliakatsos, and J. J. Abbott, Microrobots for minimally invasive medicine, Annu. Rev. Biomed. Eng **12**, 55 (2010).

[6] A. T. Chwang, T. Y. Wu, and J. Gray, A note on the helical movement of micro-organisms, Proc. Royal Soc. London, Ser. B **178**, 327 (1971).
[7] E. M Purcell, The efficiency of propulsion by a rotating flagellum, Proc. Natl. Acad. Sci. USA **94**, 11307 (1997).
[8] S. Chattopadhyay, R. Moldovan, C. Yeung, and X. L. Wu, Swimming efficiency of bacterium *Escherichia coli*, Proc. Natl. Acad. Sci. USA **103**, 13712 (2006).
[9] A. M. Leshansky, Enhanced low-Reynolds-number propulsion in heterogeneous viscous environments, Phys. Rev. E **80**, 051911 (2009).
[10] B. Darbois Texier, A. Ibarra, and F. Melo, Helical Locomotion in a Granular Medium, Phys. Rev. Lett. **119**, 068003 (2017).
[11] B. Liu, T. R. Powers, and K. S. Breuer, Force-free swimming of a model helical flagellum in viscoelastic fluids, Proc. Natl. Acad. Sci. USA **108**, 19516 (2011).
[12] S. E. Spagnolie, B. Liu, and T. R. Powers, Locomotion of Helical Bodies in Viscoelastic Fluids: Enhanced Swimming at Large Helical Amplitudes, Phys. Rev. Lett. **111**, 068101 (2013).
[13] W. R. Schneider and R. N. Doetsch, Effect of viscosity on bacterial motility, J. Bacteriol. **117**, 696 (1974).
[14] H. C. Berg and L. Turner, Movement of microorganisms in viscous environments, Nature (London) **278**, 349 (1979).
[15] V. A Martinez, J. Schwarz-Linek, M. Reufer, L. G. Wilson, A. N. Morozov, and W. C. K. Poon, Flagellated bacterial motility in polymer solutions, Proc. Natl. Acad. Sci. USA **111**, 17771 (2014).
[16] A. E. Patteson, A. Gopinath, M. Goulian, and P. E. Arratia, Running and tumbling with *E. coli* in polymeric solutions, Sci. Rep. **5**, 15761 (2015).
[17] Y. Magariyama and S. Kudo, A mathematical explanation of an increase in bacterial swimming speed with viscosity in linear-polymer solutions, Biophys. J. **83**, 733 (2002).
[18] H. C. Fu, V. B. Shenoy, and T. R. Powers, Low-Reynolds-number swimming in gels, Europhys. Lett. **91**, 24002 (2010).
[19] Y. Man and E. Lauga, Phase-separation models for swimming enhancement in complex fluids, Phys. Rev. E **92**, 023004 (2015).
[20] A. Zöttl and J. M. Yeomans, Enhanced bacterial swimming speeds in macromolecular polymer solutions, Nat. Phys **15**, 554 (2019).
[21] K. Qi, E. Westphal, G. Gompper, and R. G. Winkler, Enhanced Rotational Motion of Spherical Squirmer in Polymer Solutions, Phys. Rev. Lett. **124**, 068001 (2020).
[22] Z. Wu, Y. Chen, D. Mukasa, O. S. Pak, and W. Gao, Medical micro/nanorobots in complex media, Chem. Soc. Rev. (2020), doi: 10.1039/D0CS00309C.
[23] J. Sznitman and P. E. Arratia, Locomotion through complex fluids: An experimental view, in *Complex Fluids in Biological Systems*, edited by S. E. Spagnolie (Springer, New York, 2015), pp. 245–281.
[24] G. J. Elfring and E. Lauga, Theory of locomotion through complex fluids, in *Complex Fluids in Biological Systems*, edited by S. E. Spagnolie (Springer, New York, 2015), pp. 283–317.
[25] E. Lauga, Propulsion in a viscoelastic fluid, Phys. Fluids **19**, 083104 (2007).
[26] H. C. Fu, C. W. Wolgemuth, and T. R. Powers, Swimming speeds of filaments in nonlinearly viscoelastic fluids, Phys. Fluids **21**, 033102 (2009).
[27] J. Teran, L. Fauci, and M. Shelley, Viscoelastic Fluid Response can Increase the Speed and Efficiency of a Free Swimmer, Phys. Rev. Lett. **104**, 038101 (2010).
[28] X. N. Shen and P. E. Arratia, Undulatory Swimming in Viscoelastic Fluids, Phys. Rev. Lett. **106**, 208101 (2011).
[29] B. Thomases and R. D. Guy, Mechanisms of Elastic Enhancement and Hindrance for Finite-Length Undulatory Swimmers in Viscoelastic Fluids, Phys. Rev. Lett. **113**, 098102 (2014).
[30] B. Qin, A. Gopinath, J. Yang, J. P. Gollub, and P. E. Arratia, Flagellar kinematics and swimming of algal cells in viscoelastic fluids, Sci. Rep. **5**, 9190 (2015).
[31] E. Lauga, The bearable gooeyness of swimming, J. Fluid Mech. **762**, 1 (2015).
[32] C. Datt, L. Zhu, G. J. Elfring, and O. S. Pak, Squirming through shear-thinning fluids, J. Fluid Mech. **784**, R1 (2015).

[33] T. D. Montenegro-Johnson, D. J. Smith, and D. Loghin, Physics of rheologically enhanced propulsion: Different strokes in generalized stokes, Phys. Fluids **25**, 081903 (2013).
[34] J. R. Vélez-Cordero and E. Lauga, Waving transport and propulsion in a generalized Newtonian fluid, J. Non-Newtonian Fluid Mech. **199**, 37 (2013).
[35] G. Li and A. M. Ardekani, Undulatory swimming in non-Newtonian fluids, J. Fluid Mech. **784**, R4 (2015).
[36] D. A. Gagnon, N. C. Keim, and P. E. Arratia, Undulatory swimming in shear-thinning fluids: experiments with *Caenorhabditis elegans*, J. Fluid Mech. **758**, R3 (2014).
[37] D. A. Gagnon and P. E. Arratia, The cost of swimming in generalized Newtonian fluids: Experiments with *C. elegans*, J. Fluid Mech. **800**, 753 (2016).
[38] T. D. Montenegro-Johnson, Fake μs: A cautionary tail of shear-thinning locomotion, Phys. Rev. Fluids **2**, 081101 (2017).
[39] J. Lighthill, Flagellar hydrodynamics, SIAM Rev. **18**, 161 (1976).
[40] S. Gómez, F. A. Godínez, E. Lauga, and R. Zenit, Helical propulsion in shear-thinning fluids, J. Fluid Mech. **812**, R3 (2017).
[41] Z. Qu and K. S. Breuer, Effects of shear-thinning viscosity and viscoelastic stresses on flagellated bacteria motility, Phys. Rev. Fluids **5**, 073103 (2020).
[42] E. E. Riley and E. Lauga, Empirical resistive-force theory for slender biological filaments in shear-thinning fluids, Phys. Rev. E **95**, 062416 (2017).
[43] K. Pietrzyk, H. Nganguia, C. Datt, L. Zhu, G. J. Elfring, and O. S. Pak, Flow around a squirmer in a shear-thinning fluid, J. Non-Newton. Fluid. **268**, 101 (2019).
[44] G. J. Hancock, The self-propulsion of microscopic organisms through liquids, Proc. R. Soc. London, A **217**, 96 (1953).
[45] J. Lighthill, *Mathematical Biofluiddynamics* (SIAM, Philadelphia, 1975).
[46] J. Happel and H. Brenner, *Low Reynolds Number Hydrodynamics with Special Applications to Particulate Media* (Noordhoff, Leiden, 1973).
[47] R. B. Bird, R. C. Armstrong, and O. Hassager, *Dynamics of Polymeric Liquids, Vol. 1: Fluid Mechanics* (John Wiley, New York, 1987).
[48] S. Childress, *Mechanical of Swimming and Flying* (Cambridge University Press, Cambridge, UK, 1981).
[49] E. Lauga and T. R. Powers, The hydrodynamics of swimming microorganisms, Rep. Prog. Phys. **72**, 096601 (2009).
[50] H. Brenner, Effect of finite boundaries on the stokes resistance of an arbitrary particle, J. Fluid Mech. **12**, 35 (1962).
[51] D. F. Katz, J. R. Blake, and S. L. Paveri-Fontana, On the movement of slender bodies near plane boundaries at low Reynolds number, J. Fluid Mech. **72**, 529 (1975).
[52] M. Ramia, D.L. Tullock, and N. Phan-Thien, The role of hydrodynamic interaction in the locomotion of microorganisms, Biophys. J. **65**, 755 (1993).
[53] B. U. Felderhof, Swimming at low Reynolds number of a cylindrical body in a circular tube, Phys. Fluids **22**, 113604 (2010).
[54] B. Liu, K. S. Breuer, and T. R. Powers, Propulsion by a helical flagellum in a capillary tube, Phys. Fluids **26**, 011701 (2014).
[55] M. J. Lighthill, On the squirming motion of nearly spherical deformable bodies through liquids at very small Reynolds numbers, Comm. Pure Appl. Math. **5**, 109 (1952).
[56] H. Nganguia, K. Pietrzyk, and O. S. Pak, Swimming efficiency in a shear-thinning fluid, Phys. Rev. E **96**, 062606 (2017).
[57] Y. I. Cho and K. R. Kensey, Effects of the non-Newtonian viscosity of blood on flows in a diseased arterial vessel. Part 1: Steady flows, Biorheology **28**, 241 (1991).
[58] F. J. H. Gijsen, F. N. van de Vosse, and J. D. Janssen, The influence of the non-Newtonian properties of blood on the flow in large arteries: Steady flow in a carotid bifurcation model, J. Biomech. **32**, 601 (1999).
[59] W. G. Li, X. Y. Luo, S. B. Chin, N. A. Hill, A. G. Johnson, and N. C. Bird, Non-Newtonian bile flow in elastic cystic duct: One- and three-dimensional modeling, Ann. Biomed. Eng. **36**, 1893 (2008).
[60] H. C. Berg, The rotary motor of bacterial flagella, Annu. Rev. Biochem. **72**, 19 (2003).

[61] F. Qiu, R. Mhanna, L. Zhang, Y. Ding, S. Fujita, and B. J. Nelson, Artificial bacterial flagella functionalized with temperature-sensitive liposomes for controlled release, Sens. Actuators B Chem. **196**, 676 (2014).

[62] M. Medina-Sanchez, L. Schwarz, A. K. Meyer, F. Hebenstreit, and O. G. Schmidt, Cellular cargo delivery: Toward assisted fertilization by sperm-carrying micromotors, Nano Lett. **16**, 555 (2016).

[63] G. Chatzipirpiridis, C. de Marco, E. Pellicer, O. Ergeneman, J. Sort, B. J. Nelson, and S. Pane, Template-assisted electroforming of fully semi-hard-magnetic helical microactuators, Adv. Eng. Mater. **20**, 1800179 (2018).